

## The evolution of a supermassive retrograde binary embedded in an accretion disk

P. B. Ivanov<sup>1,2</sup> J. C. B. Papaloizou<sup>2</sup> S.-J. Paardekooper<sup>3</sup> A. G. Polnarev<sup>3</sup>

<sup>1</sup> *Astro Space Centre, P. N. Lebedev Physical Institute,  
84/32 Profsoyuznaya st., Moscow, 117997, Russia; pbi20@cam.ac.uk straiizys@itpa.lt*

<sup>2</sup> *DAMTP, University of Cambridge,  
Wilberforce Road, Cambridge CB3 0WA, UK*

<sup>3</sup> *Astronomy Unit, Queen Mary University of London,  
Mile end Road, London, E1 4NS, UK*

Received:

**Abstract.** In this note we briefly discuss the main results of a recent study of massive binaries with unequal mass ratio  $q$  for which the orbit is circular. The orbit is embedded in an accretion disk with its orbital rotation being in the opposite sense to that of the disk gas. A more complete presentation of these results is published elsewhere (Ivanov et al. 2014).

It is shown that when the mass ratio is sufficiently large the binary opens a gap in the disk. However, the mechanism of gap formation has a very different character to that applicable to the prograde case. The binary is found to migrate inwards due to interaction with the disk with a characteristic timescale,  $t_{ev}$ , of the order of  $M_p/\dot{M}$ , where  $M_p$  is the mass of the less massive component of the binary, henceforth referred to as the perturber, and  $\dot{M}$  is the accretion rate through the disk. When  $q \ll 1$  the accretion rate to the more massive component is  $\sim \dot{M}$ , while the accretion rate to the perturber is smaller, being of the order of  $q^{1/3}\dot{M}$ . However, we remark that the accretion rate to the perturber can be significantly amplified during the late stages of the orbital evolution of a supermassive binary black hole which are determined by gravitational wave emission. Additionally we estimate a typical time duration for which, both electromagnetic phenomena associated with accretion onto the perturber, and gravitational waves emitted by the binary could be detected by a future space borne interferometric gravitational wave antenna with realistic parameters.

The study should be extended to consider orbits with significant eccentricity, for which the formation of a gap through the action of torques associated with waves launched at Lindblad resonances becomes possible. Also, when the accretion disk has a non zero inclination with respect to the orbital plane of a retrograde binary at large distances, this inclination may increase on a timescale that can be similar to, or smaller than  $t_{ev}$ . This is also an aspect for future study.

**Key words:** Accretion disks: -binaries, Hydrodynamics, Galaxies: quasars: supermassive black holes, Planet-disk interactions

## 1 Introduction

Supermassive black hole binaries (SBBH) may form as a consequence of galaxy mergers, see e.g. Komberg 1968, Begelman, Blanford & Rees 1980. Since the direction of the angular momenta associated with the motion of the binary and the gas in the accretion disk is potentially uncorrelated, the binary may be on either a prograde or retrograde orbit with respect to the orbital motion in the disk when it becomes gravitationally bound and starts to interact with it.

The prograde case has been considered by many authors beginning with Ivanov, Papaloizou & Polnarev (1999), hereafter IPP, and Gould & Rix (2000). The retrograde case has received much less attention, with relatively few numerical simulations available to date, see e.g. Nixon, King & Pringle (2011) and Nixon et al. (2011). However, the retrograde case may be as generic as the prograde case when the interaction of SBBH with an accretion disk is considered. Note that although the disk is likely to be inclined with respect to the binary orbital plane initially, alignment on a length scale corresponding to the so-called alignment radius is attained relatively rapidly, the direction of rotation of the disk gas being either retrograde or prograde with respect to orbital motion, depending on the initial inclination, see e.g. IPP.

Here we review recent results to be published in detail elsewhere (Ivanov, Papaloizou, Paardekooper and Polnarev 2014, hereafter IPPP) on the evolution of retrograde SBBH. A variety of analytical and numerical techniques were employed. For simplicity, a binary in a circular orbit that was coplanar with the disk was assumed for the most part. However, the case of an eccentric binary was also briefly discussed. The main emphasis is on the case of a small mass ratio  $q$ . However, this is taken to be sufficiently large that the disk is significantly perturbed in the neighbourhood of the binary orbit.

We describe our numerical approach to the problem of the interaction of SBBH with an accretion disk in Section 2 and a simple analytical approach for calculating the orbital evolution of SBBH in Section 3. Various associated effects and phenomena are discussed in Section 4. Finally in Section 5 we summarise our results.

## 2 Numerical simulations of massive retrograde perturbers embedded in an accretion disk

In this section we consider numerical simulations for which the perturber is massive enough to significantly perturb the accretion disk <sup>1</sup> and open a surface density depression called hereafter 'a gap' in the vicinity of its orbit. For that we require mass ratio,  $q$ , of the perturber with mass  $M_p$  to the dominant mass  $M$ , to be larger than  $\sim 1.57(H/r_p)^2$ , where  $r_p$  is the radius of perturber's orbit and  $H$  is the disk semi-thickness. We consider values of  $q$  of 0.01 and 0.02 below. In some

---

<sup>1</sup>See IPPP for the opposite case of a low mass perturber, which is insufficiently massive to open a gap.

runs accretion onto the perturber is taken into account. The initial surface density was specified to be  $\propto r^{-1/2}$  and scaled so that the total mass interior to the initial orbital radius of the perturber was  $10^{-3}$  in units of the dominant central mass.

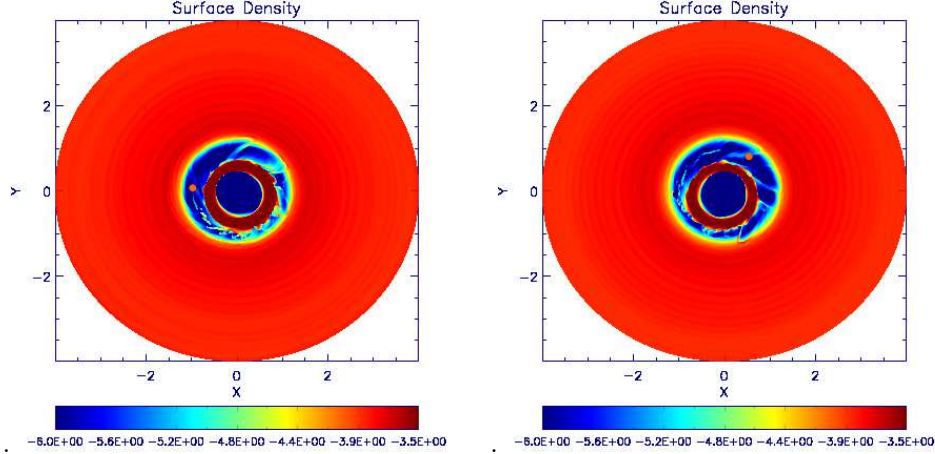


Figure 1:  $\log \Sigma$  contours for  $q = 0.02$  with softening length  $0.1H$  after 50 orbits (left panel) and after 100 orbits (right panel). In these simulations the companion, its position in each case being at the centre of the small red circle located within the gap region, was allowed to accrete. The width of the gaps slowly increases while the accretion rates, on average, slowly decrease with time. Short wavelength density waves in the outer disks are just visible. Note that values of  $\log \Sigma$  below the minimum indicated on the colour bar are plotted as that minimum value

The perturber was initiated on a retrograde circular orbit of radius  $r_0$  which is taken to be the simulation unit of length. For simulation unit of time we take the orbital period of a circular orbit with this radius. We use two different values of the softening length  $b_s$ . For the “standard case”  $b_s = 0.6H$  was adopted and the for the case of “small” softening  $b_s = 0.1H$  was adopted. For other details see IPPP.

The structure of the disk gaps for  $q = 0.02$  and  $q = 0.01$  is illustrated in the surface density contour plots presented in Figs. 1 and 2 at various times. The runs respectively correspond to the strongest and weakest gap forming cases considered in this section. Note that the gap is indeed significantly wider and deeper for  $q = 0.02$  as expected and in addition the gap edges define significantly non circular boundaries. Material crossing the gap in the form of streamers is also present. Note that an animation of the process of gap formation can be found on the website <http://astro.qmul.ac.uk/people/sijme-jan-paardekooper/publications>.

The semi-major axis is shown as a function of time for  $q = 0.02$  and  $q = 0.01$  for small softening and for  $q = 0.01$  with standard softening in Fig. 3. The behaviour depends only very weakly on whether the perturber is allowed to accrete from the disk or not. At early times the cases with  $q = 0.01$  have the migration rates

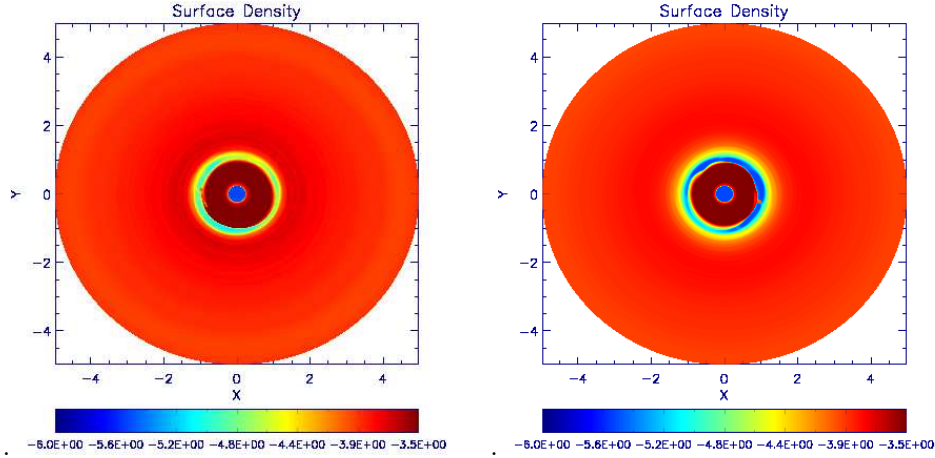


Figure 2: As in Fig. 1 but for  $q = 0.01$  with softening length  $0.6H$  after 100 orbits (left panel) and 800 orbits (right panel). As the mass ratio is lower in this case compared to that of Fig. 1 the gap in the disk is narrower. The companion, indicated by a small red circle is found in general to orbit closer to the inner disk edge at earlier times. In the left hand panel the companion grazes the inner edge slightly above the  $x$  axis for  $x < 0$ . This enhances the accretion rate at that stage.

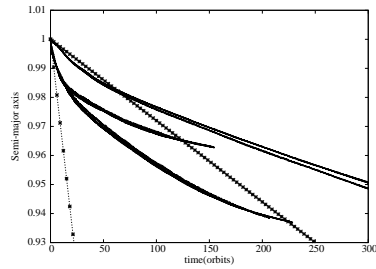


Figure 3: Semi-major axis, in units of the initial orbital radius, as a function of time for  $q = 0.02$  and  $q = 0.01$  for small softening and for  $q = 0.01$  with standard softening. Two curves without imposed crosses, which are very close together, are shown for each of these three cases. The uppermost pair of curves corresponds to  $q = 0.01$  with standard softening and the lowermost pair for  $q = 0.01$  with small softening. The central pair corresponds to  $q = 0.02$  with small softening. The lower of the pair of curves for the cases with small softening correspond to runs with accretion from the disk included. For the case with standard softening this situation is reversed. The straight lines which have imposed crosses are obtained adopting the initial Type I migration rate. The line with the more widely separated crosses corresponds to  $q = 0.01$  with small softening while the other line corresponds to  $q = 0.01$  with standard softening.

expected in the type I regime, where the gap is not open, see IPPP. However, after a few orbits the effects of gap formation become noticeable and the migration starts to slow down. For the case with  $q = 0.02$ , the initial migration rate is a factor of two smaller than the expected type I migration rate with the effects of gap formation being noticeable immediately. Note that at longer times the migration rates for  $q = 0.01$  with different softening lengths slow to become approximately equal as would be expected if the migration was governed by the viscous evolution of the disk. On the other hand, the larger open inner boundary radius adopted for the simulations with smaller softening, on account of necessary numerical convenience, results in a relatively larger angular momentum loss from the system as material passes through and this may also affect the orbital evolution (see below). In all cases the characteristic time scale becomes comparable to or greater than that for the viscous evolution of the disk.

### 3 A simple approach to evolution of the binary and the disk

A very simple approach to the problem of calculation of orbital the evolution is possible when the perturber mass is larger than a typical disk mass in a region of size  $r_p$  (see IPPP). In this case the orbital evolution timescale  $t_{ev}$  exceeds the local timescale for viscous evolution of the disk,  $t_\nu$ . After the perturber has been present in the disk for a time that is larger than  $t_\nu$ , but smaller than  $t_{ev}$ , the disk structure at radii  $r \sim r_p$  should be close to a quasi-stationary one. In this situation, the mass flux  $\dot{M}$  and the specific angular momentum at the inner disk may be assumed to be functions of time only with a characteristic time scale for change being much larger than  $t_\nu$ .

In addition, in the limit  $q \ll 1$ , the annulus in the vicinity of perturber, where impulsive interaction with the disk gas operates, is very small, with a typical dimension  $\ll r_p$ . Therefore, in the simplest treatment of the problem, we describe the influence of the perturber on the disk as providing a jump condition on the surface density, to be applied at the perturber's orbital location, in a disk otherwise evolving only under the influence of internal viscosity.

As indicated above, the mass flux through the gap is approximately constant in this limit. Furthermore, it can be easily shown (e.g. IPPP) that when the mass flux is fixed, stationary solutions depend only on one constant of integration,  $h_*$ , which is proportional to the flux of angular momentum through the disk through the relation  $\dot{L} = \dot{M}\Omega_0 r_0^2 h_*$ .

The region of the disk for which  $r$  slightly exceeds  $r_p$  should attain  $\Sigma(r_{p+}) \sim 0$  as a result of interaction with perturber, which causes disk gas at radii slightly exceeding  $r_p$  to lose angular momentum and be transferred to the inner region through the gap. This means that the flux of angular momentum through the disk at radii  $r \gtrsim r_p$ ,  $\dot{L}_+$ , should be  $\sim \dot{M}\sqrt{GM r_p}$  and we must accordingly set  $h_* = \sqrt{r_p/r_0}$ .

On the other hand, the flux of angular momentum through the inner disk, at

$r < \sim r_p$ ,  $\dot{L}_- i$ , should be equal to the angular momentum accreted per unit time by the component with the dominant mass,  $M$ . Assuming that  $r_p$  is much larger than the size of the last stable circular orbit around that component, we can set  $\dot{L}_- \approx 0$ .

Since the total angular momentum of the system is conserved and that, for small enough inner boundary radius, there is no angular momentum flux through the inner disk, the outward angular momentum flux through the outer disk,  $T$ , must be equal and opposite to the torque acting on the perturber due to the disk, the latter being  $-T$ . Thus we have

$$T \approx -\dot{M}(t)\sqrt{GM r_p} \quad (1)$$

where  $\dot{M}(t) > 0$ , and, accordingly,  $T < 0$ .

As shown in IPPP when the disk has formally infinite extent  $\dot{M}(t) \approx \text{const}$  being equal to the mass flux at infinity. In this case, using (1) and the law of angular momentum conservation we get

$$r_p = r_0 \exp(t/t_{ev}), \quad t_{ev} = \frac{M_p}{2\dot{M}}. \quad (2)$$

When the disk has a finite extent as in our numerical simulations, a simple approach to the calculation of the dependence of  $\dot{M}$  on  $t$  is possible for a disk with a constant kinematic viscosity. A comparison of the results based on analytic and numerical methods is shown in Fig. 16 of IPPP, which demonstrates excellent agreement between the methods.

## 4 Additional effects and phenomena

### 4.1 Effects of finite eccentricity

So far we have assumed that the eccentricity of the binary is zero. In this case it can be easily shown that there are no outer Lindblad resonances and the standard mechanism of gap opening by a torque carried by waves launched at resonances is absent. The situation is different, however, in case of an eccentric retrograde binary, which can be formed both when SBBH and planetary systems are considered, see e.g. Polnarev & Rees (1994), Papaloizou & Terquem (2001) for the case of SBBH and planetary systems, respectively. In this case the Lindblad resonances are present although the amplitude of the torque is suppressed compared with the prograde case. Provided the gap (or cavity) is formed through the action of the resonances, its structure is quite different from that discussed above and can resemble the prograde case discussed in IPP. Namely, the action of resonances supplies positive angular momentum to the disk gas, thus leading to accumulation of the gas at distances exceeding  $r_p$ , and accordingly, formation of gap or circumbinary cavity. In order to estimate the importance of this effect we use the theory of Goldreich & Tremaine (1979) and the gap opening criterion discussed in Lin & Papaloizou (1979) and Artymowicz & Lubow (1994). The condition of gap

formation can be formulated as the condition for the binary eccentricity to exceed some critical value  $e_{crit}^{l,m}$ , where  $l$  and  $m$  correspond to a Fourier harmonics with temporal and azimuthal mode numbers  $m$  and  $l$ , respectively. We have

$$e_{crit}^{1,-1} \approx 0.2\alpha_*^{1/4} q_*^{-1/2} \delta_*^{1/2} \quad (3)$$

and

$$e_{crit}^{2,-1} = 0.37\alpha_*^{1/6} q_*^{-1/3} \delta_*^{1/3}, \quad (4)$$

for  $m = 1, l = -1$  and  $m = 2, l = -1$ , respectively, where  $\alpha_* = \alpha/10^{-2}$ ,  $q_* = q/10^{-2}$  and  $\delta_* = (H/r)/10^{-3}$ . Since the critical eccentricities are of the order of 0.2–0.4 for very thin accretion disks, which may be present in galactic nuclei, this effect may operate there. The situation is less favourable for protoplanetary disks, where we typically have  $\delta \sim 0.05$ , and, accordingly,  $\delta_* \sim 50$ . In this case we have the critical eccentricities formally exceeding unity for  $\alpha_* = 1$ , and, therefore, this effect is unlikely to operate unless  $\alpha$  is very small.

## 4.2 Mass flux to the perturber

The mass flux to the perturber is estimated in IPPP as

$$\dot{m} \sim q^{1/3} \dot{M}. \quad (5)$$

It was also shown by IPPP that this estimate agrees with numerical simulations provided the results obtained by the numerical approach are averaged over several orbital periods. On the other hand the numerical approach shows that the mass flux can change by order of magnitude or more on the orbital timescale. Note that this variability may lead to some important consequences since it can lead to luminosity variability on the same time scale provided accretion efficiency is sufficiently large. Also note that equation (5) shows that the mass flux onto the perturber is smaller than the mass flux to the primary component provided  $q \ll 1$  and the orbital evolution is determined by the interaction with the disk. This, however, can be changed for SBBH when the orbital evolution is sped up by the emission of gravitational waves, see the next Section.

## 4.3 The influence of emission of gravitational waves on the orbital evolution and accretion rate for SBBH

In the case of SBBH there is an additional important mechanism for driving orbital evolution through emission of gravitational waves. For a circular orbit and  $q \ll 1$ , the corresponding time scale,  $t_{gw}$  can be easily obtained from expressions given by e.g. Landau & Lifshitz (1975) and from equation (2). We first remark that  $t_{ev}$  can be written as

$$t_{ev} \approx 5 \cdot 10^7 \left( \frac{q_{-2} M_8}{\dot{M}_{-2}} \right) yr, \quad (6)$$

where  $q_{-2} = q/10^{-2}$ ,  $M_8 = M/10^8 M_\odot$ , and  $\dot{M}_{-2} = \dot{M}/(10^{-2} M_\odot yr^{-1})$ . From the condition  $t_{gw} < t_{ev}$  we find that gravitational waves determine the orbital

evolution when

$$r_p < r_{gw(I)} = r_g \left( \frac{8cqt_{ev}}{5r_g} \right)^{1/4} \approx \frac{0.7q_{-2}M_8}{(M_{-2})^{1/4}} pc. \quad (7)$$

Note that the orbital period at  $r_p \sim r_{gw(I)}$  being given by  $P_{orb} \approx 5r_{-2}^{3/2}M_8^{-1/2}yr$ , where  $r_{-2} = r_p/(10^{-2}pc)$  is expected to be of the order of a few years. From the definition of  $r_{gw(I)}$  and (6) it also follows that

$$t_{gw} = \left( \frac{r_p}{r_{gw(I)}} \right)^4 t_{ev}. \quad (8)$$

Another important length scale,  $r_{gw(\nu)}$ , is determined by the condition that the time scale for orbital evolution due to gravitational radiation be less than the time scale for viscous evolution of the disk, or  $t_{gw}(r_p < r_{gw(\nu)}) < t_\nu$ . For this length scale we obtain

$$r_{gw(\nu)} = r_g \left[ \frac{32\sqrt{2}q}{15\alpha\delta^2} \right]^{2/5} \approx 5 \cdot 10^{-3} M_8 (q_{-2})^{2/5} \alpha_*^{-2/5} \delta_*^{-4/5} pc. \quad (9)$$

When  $r < r_{gw(\nu)}$ , from the point of view of the perturber, the disk gas is transferred from the inner the disk to the outer disk which is the opposite direction to that considered above. However, arguments leading to the expression (5) remain essentially the same if instead of the accretion rate through the disk,  $\dot{M}$ , the rate of transfer of the disk gas through perturber's orbit,  $\dot{M}_{tr}$ , is adopted. Note that  $\dot{M}_{tr}$  is defined in the frame, where perturber is at rest. We can estimate it as  $\dot{M}_{tr} \sim M_d(r < r_p)/t_{gw}$ , where the disk mass inside the perturber's orbit. As discussed above the disk inside the perturber's orbit may be approximated as a stationary accretion disk, characterised by the accretion rate  $\dot{M}$ , and therefore, its mass can be estimated as  $M_d(r < r_p) \sim \dot{M}t_\nu$ . Taking these considerations into account we obtain

$$\dot{m} \sim \frac{q^{1/3}M_d(r < r_p)}{t_{gw}} \sim \frac{q^{1/3}\dot{M}t_\nu}{t_{gw}} \sim \frac{q^{1/3}\dot{M}r_{gw(\nu)}^4}{r^4}. \quad (10)$$

This indicates that the accretion rate onto the secondary can exceed that onto the primary,  $\sim \dot{M}$ , provided that

$$r < r_{crit} = q^{1/12}r_{gw(\nu)}. \quad (11)$$

Since the power of  $q$  in (11) is small, we have that typically  $r_{crit} \sim r_{gw(\nu)}$ .

#### 4.4 An estimate of the time for which gravitational waves with amplitudes sufficient for possible detection will be emitted during inspiral

Let us assume that the future space-borne gravitational wave antenna will have sensitivity  $h_0 = 10^{-22}\tilde{h}_{-22}$  in the frequency range

$$\omega_{min} = 10^{-5} \tilde{\omega}_{-5} Hz < \omega_{gw} < \omega_{max} = 10^{-2} \tilde{\omega}_{-2} Hz \quad (12)$$



where  $\tilde{h}_{-22} = h_0/10^{-22}$ ,  $\tilde{\omega}_{-5} = \omega_{min}/10^{-5}Hz$ ,  $\tilde{\omega}_{-2} = \omega_{max}/10^{-2}Hz$  are dimensionless constants, and we expect the antenna to be sensitive to gravitational waves with a typical amplitude  $10^{-22}$  and typical frequencies  $10^{-5} - 10^{-2}Hz$ . On the other hand, when SBBH orbit is approximately circular we have

$$\omega_{gw} \approx 2\omega_{orbit} = 2(GM)^{1/2}r^{-3/2} \text{ and hence } r = r_g(c\sqrt{2}/r_g\omega_{gw})^{2/3}. \quad (13)$$

From (13) and the conditions on  $\omega_{gw}$  given by (12) one obtains the following constraints on the orbital radius during this final stage:

$$\beta_{min} < r/r_g < \beta_{max}, \text{ where } \beta_{min} = \left(\sqrt{2}r_g\omega_{max}/c\right)^{-2/3}$$

$$\text{and } \beta_{max} = \left(\sqrt{2}r_g\omega_{min}/c\right)^{-2/3}. \quad (14)$$

Another constraint is obtained from a comparison of the amplitude of the emitted gravitational waves,  $|h_{\alpha\beta}|$ , with  $h_0$ . Using the quadrupole formula (Landau & Lifshitz, 1975) to make an order of magnitude estimate, one obtains

$$h \sim (2G/3c^4L)\ddot{D}_{\alpha\beta} \sim (2G/3c^4L)(3/2)qMr^2\omega_{gw}^2$$

$$= (G/c^4L)qMr^2(4GM)/r^3 = qr_g^2/rL > h_0, \quad (15)$$

where  $L = L_{100} \times 100$  Mpc is the distance to the binary and  $\ddot{D}_{\alpha\beta}$  is the second time derivative of the quadrupole tensor. Noting that  $r > r_{st} = 3r_g$ , where  $r_{st}$  is the radius of the last stable circular orbit for the Schwarzschild metric, the conditions for the gravitational radiation from the binary to be detectable can be written in the form

$$\max[3, \beta_{min}] < \frac{r}{r_g} < \min[\beta^*, \beta_{max}], \text{ where } \beta^* = \frac{qr_g}{h_0L}. \quad (16)$$

These constraints are compatible if

$$\beta^* > 3, \beta^* > \beta_{min} \text{ and } \beta_{max} > 3. \quad (17)$$

The above inequalities can be rewritten as

$$q_{-2} > 3 \times 10^{-9}\tilde{h}_{-22}L_{100}M_8^{-1}, \quad q_{-2} > 3 \times 10^{-10}\tilde{h}_{-22}L_{100}M_8^{-5/3}\tilde{\omega}_{-2}^{-2/3}$$

$$\text{and } M_8 < 3 \times 10^2\tilde{\omega}_{-5}^{-1}. \quad (18)$$

In the most realistic case

$$q_{-2} > 3 \times 10^{-8}\tilde{h}_{-22}L_{100}M_8^{-5/3}\tilde{\omega}_{-5}^{-2/3}, \text{ which corresponds to } \beta^* > \beta_{max} \quad (19)$$

and the duration of this final stage is

$$\Delta t_{gw} \approx 10^2 q_{-2}^{-1} M_8^{-5/3} \tilde{\omega}_{-5}^{-8/3} \text{ yr.} \quad (20)$$

During this period the frequency of gravitational waves increases from  $\omega_{min}$  to  $\omega_*$ , where

$$\omega_* = \omega_{max}, \text{ if } M_8 < 3 \times 10^{-2} \tilde{\omega}_{-2}^{-1} \text{ (which corresponds to } \beta_{min} > 3) \quad (21)$$

$$\text{or } \omega_* = 3 \times 10^{-4} M_8^{-1} Hz \text{ (the frequency corresponding to } r = r_{st} = 3r_g),$$

$$\text{if } 3 \times 10^{-2} \tilde{\omega}_{-2}^{-1} < M_8 < 3 \times 10^2 \tilde{\omega}_{-5}^{-1} \text{ (corresponding to } \beta_{min} < 3 < \beta_{max}). \quad (22)$$

## 5 Conclusions

In this note we briefly reviewed results obtained in IPPP on the interaction of a retrograde circular binary with a coplanar accretion disk. We discussed the following results.

1) When the mass ratio  $q$  is small, but larger than  $\sim 1.6(H/r_p)^2$  a gap in the vicinity of the perturber opens due to increase of radial velocity of the gas in this region. Its size smaller than the orbital distance  $r_p$  in this limit.

2) For such systems assuming that perturber's mass is larger than a typical disk mass at distances  $\sim r_p$  the disk structure outside the gap is close to a quasi-stationary one. The inner disk has nearly zero angular momentum flux, while the outer disk has angular momentum flux equal to the mass flux times the binary specific angular momentum. The orbital distance evolution timescale  $t_{ev} = M_p/(2\dot{M})$  is determined by the law of conservation of angular momentum. Note that this picture differs from the prograde case with similar parameters, where there is a pronounced cavity instead of the inner disk and the orbital evolution is somewhat faster.

3) When the orbital evolution is determined by the interaction with the disk the mass flux onto the more massive component  $\sim \dot{M}$ , while the average mass flux onto the perturber is smaller  $\sim q^{1/3}\dot{M}$ . However, the latter exhibits strong variability on timescales on the order of the orbital period. The mass flux to the perturber can increase significantly during the late stages of the inspiral of SBBH when the emission of gravitational waves controls the orbital evolution.

4) When the binary is sufficiently eccentric and the disk is sufficiently thin, the opening of a 'conventional' cavity within the disk is also possible due to the presence of Lindblad resonances.

Additionally, we estimated a time duration for which the emitted gravitational waves would have sufficient amplitude for detection by a space-borne interferometric gravitational wave antenna with realistic parameters. This is given by eq. (20) as well as the appropriate range of frequencies as a function of the primary black hole mass.

Note that all these results have been obtained under the assumption that the binary orbit and the disk are coplanar. This may break down at late times since

IPPP provide an estimate that their mutual inclination angle measured at large distances grows with time for the case of a retrograde binary. The typical timescale is on the order of, or possibly even smaller than,  $t_{ev}$  depending on the mass ratio and disk parameters. Thus, this effect should be taken into account in future studies of these systems.

ACKNOWLEDGMENTS. PBI was supported in part by programme 22 of the Russian Academy of Sciences and in part by the Grant of the President of the Russian Federation for Support of Leading Scientific Schools of the Russian Federation NSh-4235.2014.2.

#### REFERENCES

- Artymowicz, P., Lubow, S. H., 1994, *ApJ*, 421, 651  
Begelman, M. C., Blandford, R. D., Rees, M. J., 1980, *Nature*, 287, 307  
Goldreich, P., Tremaine, S., 1979, *ApJ*, 233, 857  
Gould, A., Rix, H.-W., 2000, *ApJ*, 532L, 29  
Ivanov, P. B., Papaloizou, J. C. B., Polnarev, A. G., 1999, *MNRAS*, 307, 79  
Ivanov, P. B., Papaloizou, J. C. B., Paardekooper, S.-J., Polnarev, A. G., 2014, *astro-ph 1410.3250*, *A&A*, accepted  
Landau, L. D., Lifshitz, E. M., 1971, *The Classical Theory of Fields ( Volume 2 of A Course of Theoretical Physics )*, Pergamon Press  
Komberg, B. V., 1968, *Soviet Astronomy*, 11, 727  
Lin, D. N. C., Papaloizou, J., 1979, *MNRAS*, 188, 191  
Nixon, C. J., King, A. R., Pringle, J. E., 2011, *MNRAS*, 417, L66  
Nixon, C. J., Cossins, P. J., King, A. R., Pringle, J. E., 2011, *MNRAS*, 412, 1591  
Papaloizou, J. C. B., Terquem, C., 2001, *MNRAS*, 325, 221  
Polnarev A. G., Rees, M. J., 1994, *A&A*, 283, 301